JOURNAL OF SOLID STATE CHEMISTRY **126,** 227–234 (1996)
ARTICLE NO. 0333

Energy Positions of Oxide Semiconductors and Photocatalysis with Iron Complex Oxides

Yasumichi Matsumoto

Department of Applied Chemistry, Faculty of Engineering, Kumamoto University, Kurokami 2-39-1, Kumamoto 860, Japan

Received April 19, 1996; in revised form July 18, 1996; accepted July 23, 1996

Energy position, bandgap, band structure, and their relationships were reviewed for various oxide semiconductors, especially iron oxides, in photoelectrochemistry and photocatalysis, and the photocatalytic reduction of CO_2 on some iron complex oxides was demonstrated. A linear relationship between bandgap and band edge was obtained for almost all the semiconductor oxides. It was pointed out that a bandgap energy higher than about 2.46 eV is necessary for water photolysis without bias voltage. It was found that the energy positions of the band edge can be controlled by the electronegativity of the metal elements constituting the iron complex oxides. The relationship between the band structure and the charge transfer site was also examined. The photocatalytic reduction of CO_2 to CH_3OH was demonstrated for $CaFe_2O_4$ and Fe–Bi–Sr–Pb–O complex oxides. The photocatalytic activity of the latter oxide with a layer structure increased with increased Pb content. The catalytic mechanism was discussed from the point of view of the redox mechanism as well as the energy position of the band edge. © 1996 Academic Press, Inc.

INTRODUCTION

Some oxide semiconductors act as a photoelectrode in photoelectrochemistry and/or a photocatalyst, and a large number of papers on the photoelectrochemical behavior have already been published for oxide semiconductors. The energy positions of the conduction band and the valence band edges are well-known to be very important for photoelectrode reactions and photocatalytic activities. There are some papers (1–3) suggesting various relationships between the energy positions of the band edges, the bandgap, the electronegativity of the oxide, and the band structure of the oxide. However, clear conclusions about these relationships have not been derived from theory involving the band structure.

Complex oxides containing more than two kinds of metal ions will be very important for photoelectrochemistry and photocatalysis because of their interesting chemical and physical properties. For example, some niobium oxides with a layer structure (4) and some complex iron oxides (5) show interesting photocatalytic properties. Therefore, some parameters for photocatalysis and photoelectrochemistry such as the band edge energies will need to be predicted for the complex oxides.

In the present paper, the band structure of the oxide semiconductors and their energy positions are discussed from the point of view of the prediction of photocatalytic activity. Especially, iron complex oxides having a relatively small bandgap are discussed in detail, and the photocatalysis by the iron oxides with a layer structure is demonstrated for methanol production from carbon dioxide reduction.

BAND STRUCTURE AND ENERGY POSITIONS FOR OXIDE SEMICONDUCTORS

Relationship between Band Edge Energies and Bandgap

The band structure and the energy position of an *n*-type oxide semiconductor in solution are illustrated in Fig. 1. A reversible hydrogen electrode (RHE) was used as the reference because pH dependence of the flatband potential of the oxide can be neglected (pH dependence for both the flatband potential of the oxide and RHE are 60 mV/pH). EA, IP, Ef, Eg, and ΔE are the electron affinity, ionization potential, Fermi level, bandgap, and energy difference between the bottom of the conduction band and Ef in the bulk oxide, respectively. On the other hand, Efb, Ec, and Ev are the flatband potential, the conduction band edge, and the valence band edge (vs RHE) in the solution, respectively. A *p*-type oxide semiconductor has the same band structure as that of Fig. 1 except for ΔE (ΔE for a *p*-type semiconductor is the energy difference between the top of the valence band and the Fermi level). Consequently, Ec and Ev can be calculated from Efb, ΔE, and Eg.

Flatband potentials have already been measured for many oxide semiconductors but not for ΔE. In general, ΔE values are about 0.1, 0.2, 0.3, and 0.4 eV for <10, 10^2, 10^3, and $>10^4$ Ω cm in conductivity for the oxide semiconductors (6, 7), respectively. If the conductivity has not been measured, ΔE was assumed to be 0.2 eV for the calculation of Ec and Ev. The energy positions of Efb vs RHE were

0022-4596/96 $18.00
Copyright © 1996 by Academic Press, Inc.
All rights of reproduction in any form reserved.

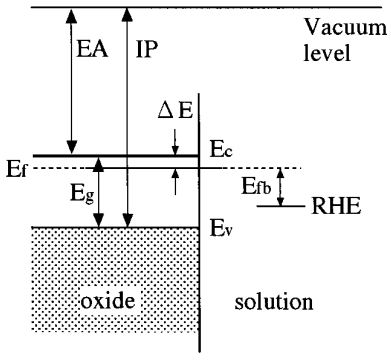

FIG. 1. Model of the surface/solution interface.

also recalculated from the Efb data vs other references. The relationship between Ec, Ev, and Eg of *n*-type oxide semiconductors calculated from the data in many references (1–3, 7–27) are illustrated in Fig. 2 (Table 1 lists the oxides used in the plots in Figs. 2 and 4). Ec and Ev, as a matter of course, must have some errors larger than 0.1 eV because of the above assumption of ΔE and the experimental errors in Efb. Moreover, specific adsorption of some ions on the oxide surface may affect both Ec and Ev. In spite of these errors, an important relationship exists for these parameters, with the exception of some transition metal oxides having filled or partly filled *d* orbitals, as shown in Fig. 2.

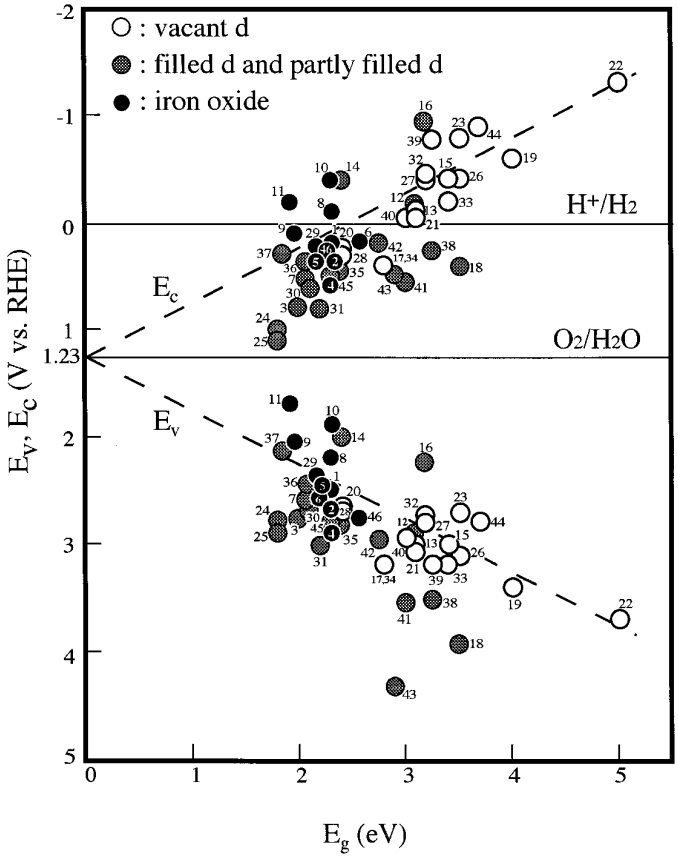

FIG. 2. Relationship between the band edge and the bandgap of oxide semiconductors.

TABLE 1
Oxide Number in Figs. 2 and 4

No.	Oxide	Ref.	No.	Oxide	Ref.
1	Fe_2TiO_5	3, 11	24	$Hg_2Nb_2O_7$	15
2	$FeTa_2O_6$	3	25	$Hg_2Ta_2O_7$	15
3	$Ti_{0.68}V_{0.32}O_2$	10, 24	26	$KTaO_3$	16
4	$CdFe_2O_4$	15	27	$SrTiO_3$	16
5	Fe_2O_3	15	28	$Pb_2Ti_{1.5}W_{0.5}O_{6.5}$	15
6	$YFeO_3$	14	29	$FeTiO_3$	2, 11
7	$CdSnO_3$	12	30	CdO	15
8	$Zn_{1.5}Fe_{1.0}Ti_{0.5}O_4$	7	31	$LuRhO_3$	3
9	$ZnFe_2O_4$	7	32	$La_2Ti_2O_7$	8
10	Sr_2FeNbO_6	19	33	Nb_2O_5	15
11	$Sr_3FeNb_2O_9$	19	34	Bi_2O_3	21
12	ZnO	1	35	In_2O_3	22
13	TiO_2	16	36	$CuWO_4$	20
14	$Cr_2Ti_2O_7$	3	37	Cu_3WO_6	20
15	$NaNbO_3$	23	38	$Bi_{12}GeO_{20}$	9
16	Zn_2TiO_4	7	39	$Bi_{12}SiO_{20}$	17
17	PbO	25	40	Sb_2O_3	3
18	SnO_2	16	41	NbO_2	10
19	Ta_2O_5	15	42	$Ti_{0.8}Nb_{0.2}O_2$	10
20	WO_3	18	43	$Ti_{0.5}Nb_{0.5}O_2$	10
21	$BaTiO_3$	15	44	$SrNb_2O_6$	3
22	ZrO_2	15	45	Cd_2SnO_4	3
23	$CaTiO_3$	3	46	$PbFe_{12}O_{19}$	13

The relationship between Ec, Ev, and Eg can be roughly represented by the following equations:

$$\text{Ec (V vs RHE)} = 1.23 - \text{Eg (eV)}/2 \quad [1]$$

$$\text{Ev (V vs RHE)} = 1.23 + \text{Eg (eV)}/2. \quad [2]$$

These equations indicate that a bandgap higher than about 2.46 eV is necessary for water photolysis without bias voltage. The valence band and the conduction band mainly consist of the p-band formed by the p orbital of the oxygen anion and the d and/or s-bands formed by the d and/or s orbitals of the transition metal cation in the oxide, respectively, if the d orbital is vacant. The relationship of Eq. [2] disagrees with that reported by Scaife (3), where the p-band was fixed in energy position. The valence band will be formed by the d orbital in some cases, when the transition metal cation has filled or partly filled d orbital. On the other hand, the conduction band is formed by the d and/or s orbital independent of the filled or partly filled d orbital. This will be the reason that the relationship of Eq.

[1] for Ec, rather than Eq. [2] for Ev, roughly holds for all oxides, as shown in Fig. 2.

Figure 3 shows a general model of the band formation for the oxide. The energy position will be determined mainly by the Madelung energy, the electron affinity of oxygen, and the ionization potential of the transition metal in the case of an oxide containing no other metal cations such as an alkaline earth element, although the other parameters also significantly affect the energy position as shown in Fig. 3. Because the electron affinity of the oxygen anion is fixed for all the oxides, the energy positions of the band edges will be determined mainly by the bandgap if the energy difference in the ionization potentials of the metal cations is relatively small compared with the Madelung energy. This assumption will be in harmony with the result in Fig. 2 where the band edge energies, Ec and Ev, are controlled mainly by the bandgap. However, the reason the converged point is near 1.23 V for the oxides cannot be explained. Probably, this will be related to the energy position of the oxygen anion constituting all the oxides.

Relationship between Band Edge Energy, Electron Affinity, and Ionization Potential of the Iron Oxides

The energy positions of the band edges Ec and Ev are also significantly affected by other factors for the oxides containing *d*-electrons as shown in Fig. 2, although the effect of the bandgap on the energy positions is dominant. The effect of the other factors on the energy positions will be remarkable for the iron oxides where the bandgap is almost the same for all samples, i.e., 1.9–2.3 eV. Butler and Ginley showed the importance of the electronegativity of the element constituting the oxides in the energy position (2), where the work function of the element was mainly used in the calculation of the electron affinity EA and the ionization potential IP of the oxide semiconductors. Figure 4 shows the Ec and Ev as functions of EA and IP, respectively, for the various iron oxides, where the EA and IP were calculated by the Butler and Ginley method (2). The energy positions of Ec and Ev are importantly related to the EA and IP as shown in this figure. Moreover, the value of the intercept of the straight line with the vertical line is in the potential range from −4.5 to −5.0 V vs RHE. This value corresponds to that of the vacuum level and is close to −4.75 V vs SCE as reported by Lohmann (28), although the energy position of SCE depends on pH (60 mV/pH) in Fig. 4. These results indicate that the Butler and Ginley method is very useful for the prediction of the energy positions of Ec and Ev when the bandgap is almost the same. The energy positions of the bands shift to higher energies if an element low in the electronegativity (low work function) exists in the lattice of the complex oxide such as a perovskite, and vice versa, because the bandgap of the oxide is determined mainly by the transition metal cation, as stated later. For example, the energy positions of Ec and Ev of a complex iron oxide shift to higher energies (negative in electrode potential), with little change in the bandgap, when the oxide contains many alkaline or alkaline earth cations (low work function) in its composition. Consequently, the energies of the band edges can be easily

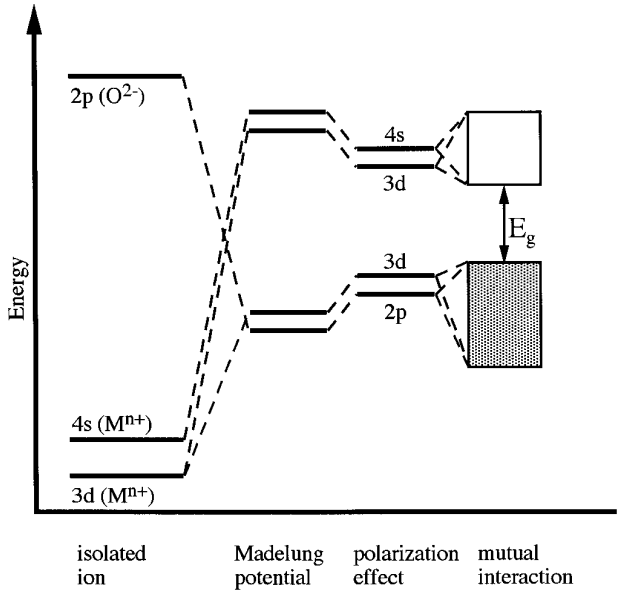

FIG. 3. Model of the band formation of an oxide semiconductor.

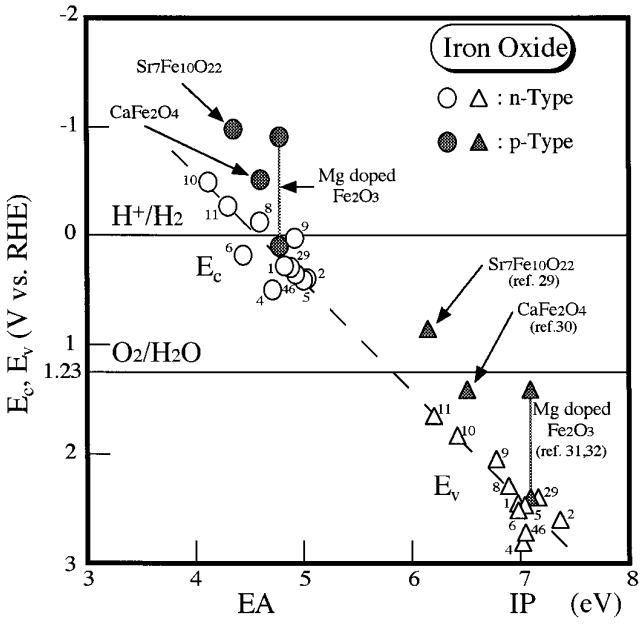

FIG. 4. Band edge energy as a function of electron affinity and ionization potential of the iron complex oxide.

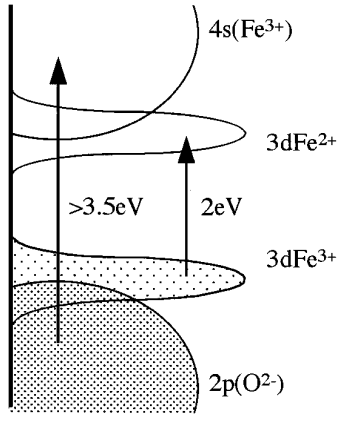

FIG. 5. Band structure of iron oxide.

controlled by the incorporation of other elements into the transition metal oxides, when the bandgap is fixed by the transition metal cation.

Band Structure of Iron Oxides

The valence band and conduction band of a 3*d*-transition metal oxide, in general, consists mainly of the 2*p* band of the oxygen anion and the 4*s* band of the transition metal anion, respectively. However, the 3*d* band will be important when it is partially filled as stated already. This band will be located in the energy position between the 4*s* and 2*p* bands. Therefore, the valence band will be the 2*p* or 3*d* band (t_{2g} band in the crystal field in an octahedral situation surrounded by an oxygen anion) in some cases.

Iron oxides consisting of Fe^{3+} ions have relatively complex band structures even in the case of a simple model. There are two typical models for the band-to-band transition for iron oxides. The first is a charge transfer model between the neighboring Fe^{3+} ions (33), where the electron transfer occurs between 3*d* bands. The second is the transition from the 3*d* band to the 4*s* band (34). As a matter of course, these transitions are strongly related. Consequently, a general band structure model for the iron oxides containing Fe^{3+} ions surrounded octahedrally by oxygen anions should be considered for the electron transition as illustrated in Fig. 5. In this model, the bandgap is about 2 eV between the 3*d* bands, and the energy transition from the 2*p* band to the 4*s* band will need an energy larger than about 3.5 eV (33). Thus, about 2 eV in the bandgap of the iron oxide semiconductors measured in photochemistry is based on the 3*d* band transition between the Fe^{3+} ions. In the case of complex iron oxides, other metal cations will scarcely affect the band structure illustrated in Fig. 5 if they are not transition metal cations. Consequently, the *d* orbitals of the Fe^{3+} ions will be very important for the photocatalysis, although the carrier mobilities are relatively low because of the narrow *d* band.

General Charge Transfer Site

There will be two electron charge transfer sites on the surface of the transition metal oxide, if other factors such as surface state are negligible. One is the transition metal cation and the other is the oxygen anion. These charge transfer sites will be easily predictable from the band structure. This prediction has already been made for the charge transfer in the oxygen electrode reaction (35). The important site is a transition metal cation for the electron transfer from the oxide to a reactant independent of the photochemistry and electrochemistry because the conduction band of the transition metal oxide consists of the 4*s* band and/or the *d* band of the transition metal cation. On the other hand, the important site is an oxygen anion or a transition metal cation for hole transfer from the oxide to a reactant (that is, electron transfer from a reactant to the valence band). Thus, the charge transfer site significantly depends on the band structure.

Figure 6 illustrates the charge transfer on the surface of the transition metal oxides. (A) corresponds to the case

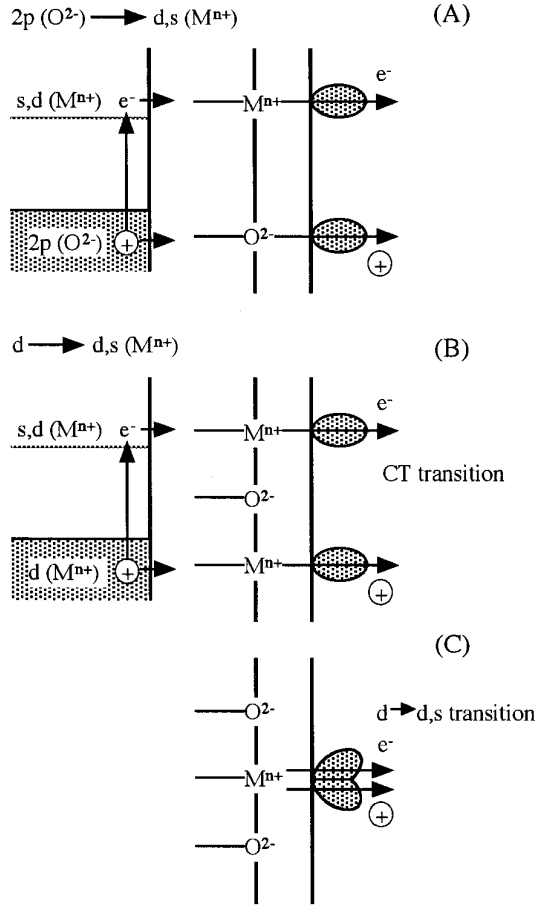

FIG. 6. Charge transfer site at the surface of an oxide semiconductor.

for an oxide having a *p*-valence band and a *d*- or *s*-conduction band. In this case, the charge transfer sites are the transition metal cation and the oxygen anion for the electron and hole, respectively. (B) and (C) correspond to the case for an oxide having a *d*-valence band and a *d*- or *s*-conduction band. In these cases, both charge transfer sites for the electron and hole are the transition metal cations. However, the sites are different transition metal cations in the case of (B) while the site is the same transition metal cation in the case of (C). The former case is due to the charge transfer between transition metal cations in the oxide, while the latter case is due to a *d*–*d* transition such as the t_{2g}–e_g transition or the *d*–*s* transition at one transition metal cation in the oxide. The charge transfer site for the iron oxide after excitation by illumination with about 2 eV corresponds to the case of either (B) or (C). However, the oxygen anion may also act as a hole transfer site in the case of photoreaction under illumination with light of higher energy than about 3.5 eV, because the hole is created in the *p*-band in this case as illustrated in Fig. 5. Consequently, sites of both the iron cation and oxygen anion must be considered for the charge transfer sites under illumination with high energy light.

PHOTOCATALYTIC REDUCTION OF CO_2 ON IRON OXIDES

Experimental

Various iron complex oxides listed in Table 2 were prepared by a conventional ceramic technique. The starting materials were the corresponding oxides and carbonates. These materials were mixed and then heated at temperatures from 850 to 1200°C. After remixing the products, the samples were pressed and then heated at the same temperatures in order to prepare disk electrodes. Ohmic contacts were made using sputtered Pt and evaporated In for the *p*-type samples and the *n*-type samples, respectively. The flatband potential and the bandgap were electrochemically measured. In these measurements, the solution was 1 *M* KOH and the reference electrode was Hg/HgO. The flatband potentials were obtained from the point of change from anodic photocurrent to cathodic photocurrent. The bandgaps were measured from the dependence of the photocurrent on the wavelength of the light.

The photocatalytic reduction of CO_2 was carried out by the following experiment. The catalyst powder suspension, which consists of 0.3 g of sample in 60 ml of 0.01 *M* NaOH saturated with CO_2 gas, was stirred in a quartz beaker using a magnetic stirrer under illumination with a 500-W ultra-high-pressure mercury lamp at room temperature. CH_3OH, CO, and some organic compounds produced in the solution were mainly analyzed by gas chromatography (FID, Porapack Q, N_2 carrier gas for CH_3OH; TCD, molecular sieve 5A for CO), while HCOOH and HCOH were analyzed by colorimetric analysis using chromotropic acid.

RESULTS AND DISCUSSION

Energy Position of the Band and Photocatalytic Activity

Table 2 lists the various iron complex oxides and their properties. Many complex iron oxides containing alkaline earth elements show a *p*-type semiconducting property, and their bandgaps were from about 1.8 to 2.2 eV. These results indicate that the band structure is based on the octahedral Fe^{3+}–O^{2-} bond and that a small amount of Fe^{4+} ion created from many Fe^{3+} ions acts as an acceptor.

Some iron oxides showed electrochemical photoresponse and photocatalytic activity for the reduction of CO_2 to CH_3OH. Both the photoresponse and photocatalytic activity are not always related as listed in Table 2. It should be noted that the materials showing electrochemical photoresponse do not always show photoreduction of CO_2 to CH_3OH. One of the important parameters for photocatalytic activity will be the energy positions of the band edges. The energy positions of some oxides listed in Table 2, which were calculated from the flatband potential measured, are shown in Fig. 7. Some redox levels related to the CO_2 reduction are also shown in Fig. 7.

The conduction and valence band edges have to be higher than the redox level for H_2CO_3 (dissolved CO_2)/CH_3OH and lower than that for O_2/H_2O, respectively, for the purpose of the charge transfer of both electrons and holes in CH_3OH and O_2 production. $CaFe_2O_4$ and the oxides with a layer structure such as $(Bi, Pb)_2Sr_2BiFe_2O_{9+y}$ satisfy both of the above conditions as shown in Fig. 7. The conduction band edge is not necessary higher than the redox level of CO_2/CO_2^- for the production of CH_3OH, because some organic compounds can be produced by the CO_2 reduction on the photocatalysts whose conduction band edges are lower than the CO_2/CO_2^- level (5, 36). $CaFe_2O_4$ and some samples of the layer oxides directly produced CH_3OH by CO_2 photoreduction. However, the other oxides with a layer structure produced to no CH_3OH, even if they satisfied both of the above conditions in energy position.

$CaFe_2O_4$ Photocatalyst

The $CaFe_2O_4$ photocatalyst satisfies two conditions in the band edge energy. In fact, CH_3OH was produced by CO_2 photoreduction on this catalyst (5). Figure 8 shows the amount of CH_3OH produced by the photoreduction of CO_2 on the Ca–Fe–O system. The starting materials were Fe_2O_3 and $CaCO_3$ for the preparation of various

TABLE 2
Properties of Various Iron Oxides

Oxide	Conductivity (400°C) ($\Omega^{-1} \cdot cm^{-1}$)	Type of semiconductor	Photoresponse[a]	Nominal valence	Eg (eV)	CO_2 photoreduction activity[b]
α-Fe_2O_3	6.5×10^{-4}	N	○	Fe^{3+}	2.2	×
$MgFe_2O_4$	2.0×10^{-6}	N	○	Fe^{3+}	2	○
$CaFe_2O_4$	7.0×10^{-3}	P	○	Fe^{3+}	1.9	○
$Ca_2Fe_2O_5$	1.0×10^{-3}	P	×	Fe^{3+}	—	×
$SrFe_{12}O_{19}$	2.0×10^{-5}	P	×	Fe^{3+}	—	×
$Sr_7Fe_{10}O_{22}$	1.6×10^{-1}	P	○	Fe^{3+}	1.8	○
$SrFeO_{2.83}$	2.0×10^{-2}	P	×	Fe^{4+}, Fe^{3+}	—	×
$Sr_3Fe_2O_{6.16}$	4.0×10^{-6}	P	○	Fe^{3+}, Fe^{4+}	—	×
$BaFe_{12}O_{19}$	1.5×10^{-2}	N	×	Fe^{3+}	—	×
$BaFe_2O_4$	$<10^{-7}$	P	○	Fe^{3+}	—	○
$BaFeO_{2.5}$	9.0×10^{-7}	P	×	Fe^{3+}	—	×
$Ba_{0.5}Ca_{0.5}Fe_2O_4$	$<10^{-7}$	P	×	Fe^{3+}	—	○
$Ba_{0.9}K_{0.1}Fe_2O_4$	$<10^{-7}$	P	×	Fe^{3+}, Fe^{4+}	—	×
$ZnFe_2O_4$	5.0×10^{-2}	N	○	Fe^{3+}	1.9	×
$Bi_{1.5}Pb_{0.5}Sr_2BiFe_2O_{9.25}$	2.0×10^{-2}	P	○	Fe^{3+}	1.8	×
$Pb_2Sr_2BiFe_2O_{9+y}$	6.0×10^{-1}	P	○	Fe^{3+}	2	○
$Bi_2Sr_2BiFe_2O_{9+y}$	5.0×10^{-2}	P	○	Fe^{3+}	1.9	×
$Bi_{1.5}Pb_{0.5}Sr_4Fe_2O_{10.04}$	3.0×10^{-1}	P	×	Fe^{3+}, Fe^{4+}	—	○

[a] ○ and × denote photoresponse and no photoresponse in electrochemistry, respectively.
[b] ○ and × denote activity and no activity in photoreduction of CO_2.

samples. The samples were prepared by heating at about 1150°C. The products were Fe_2O_3, $CaFe_2O_4$, and $Ca_2Fe_2O_5$, depending on the starting composition. Therefore, the amounts of the products shown in Fig. 8 were estimated from the starting atomic ratio of Ca/Fe and the kind of the product. The maximum of the amount of the produced CH_3OH was obtained with the composition of $CaFe_2O_4$. Thus, only $CaFe_2O_4$ acts as a photocatalyst for the reduction of CO_2 to CH_3OH.

Iron Complex Oxides with Layered Structure

There are two typical structures for an iron complex oxide with a layered structure (37,38), $(Bi,Pb)_2Sr_2BiFe_2O_{9+y}$ and $Bi_{1.5}Pb_{0.5}Sr_4Fe_2O_{10}$. The former structure is illustrated in Fig. 9. These samples also satisfy two conditions in the energy position of the band edges as shown in Fig. 7. The band positions show little dependence on the composition. Some samples show photocatalytic activity for the production of CH_3OH by photoreduction of CO_2, but the other samples show no photocatalytic activity. This result indicates that other factors as well as the energy positions of the band edges are also important for photocatalytic activity. Figure 10 shows the amount of CH_3OH as a function of the illumination time on $Bi_{0.5}Pb_{1.5}Sr_2BiFe_2O_{9+y}$ catalyst. The production of CH_3OH linearly increases with the illumination time. The Pb^{2+} ion in the

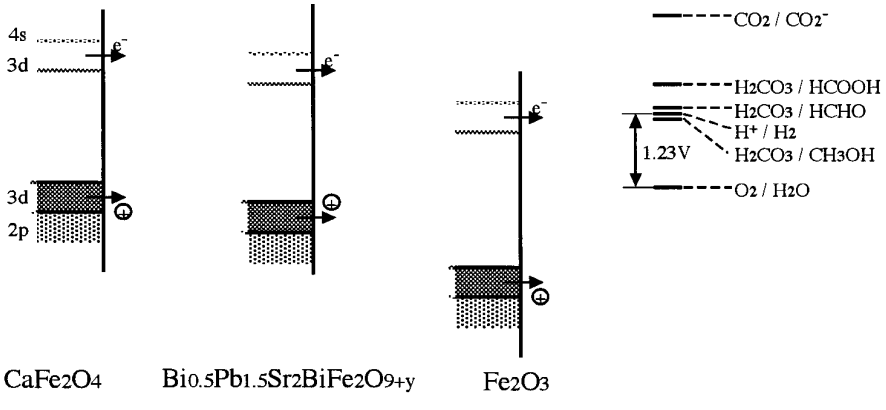

FIG. 7. Energy position of iron complex oxides.

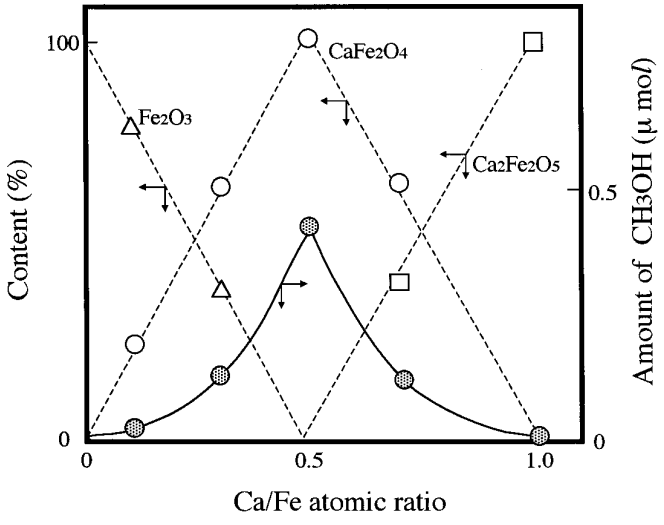

FIG. 8. Content of the iron oxide products and amount of CH_3OH produced from CO_2 (4 h illumination time) as a function of the Ca/Fe atomic ratio in the starting composition.

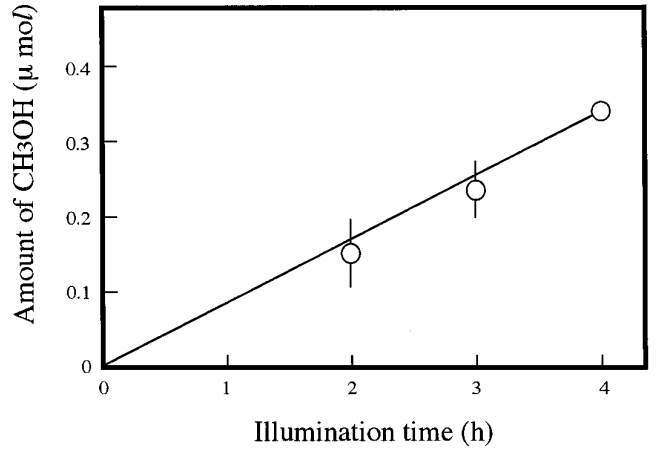

FIG. 10. Amount of CH_3OH produced from CO_2 as a function of the illumination time on $Bi_{0.5}Pb_{1.5}Sr_2BiFe_2O_{9+y}$ catalyst.

layer will be very important for photocatalytic activity. Figure 11 shows the CH_3OH production as a function of the amount of Pb in $(Bi, Pb)_2Sr_2BiFe_2O_{9+y}$. Probably, Pb^{2+} may be oxidized to Pb^{3+} or Pb^{4+} by a hole produced in the Fe–O layer, and then water is oxidized to oxygen. On the other hand, an electron produced in the Fe–O layer will directly reduce CO_2 to CH_3OH. However, some detail experiments will be necessary for clarification of the mechanism.

CONCLUSIONS

A linear relationship was found between the band edges and the bandgap of oxide semiconductors. The following equations for these parameters were essentially retained:

$$Ec\ (V\ vs.\ RHE) = 1.23 - Eg\ (eV)/2$$

$$Ev\ (V\ vs.\ RHE) = 1.23 + Eg\ (eV)/2.$$

The above relationships were discussed based on the band formation in the oxide. The energy positions of the band edges were controlled by the elements constituting the iron complex oxides. The energy position shifts to high when

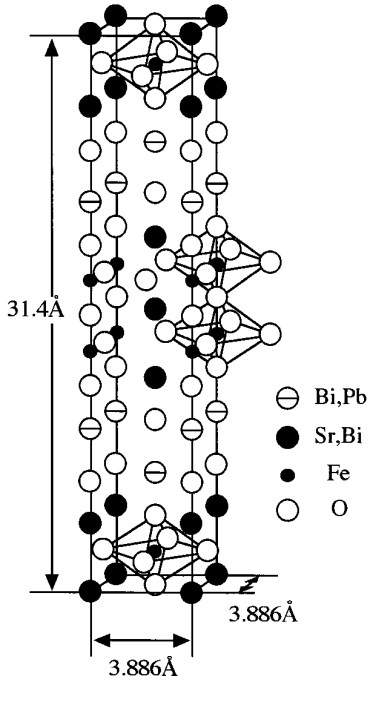

FIG. 9. $(Bi, Pb)_2Sr_2BiFe_2O_{9+y}$ crystal structure.

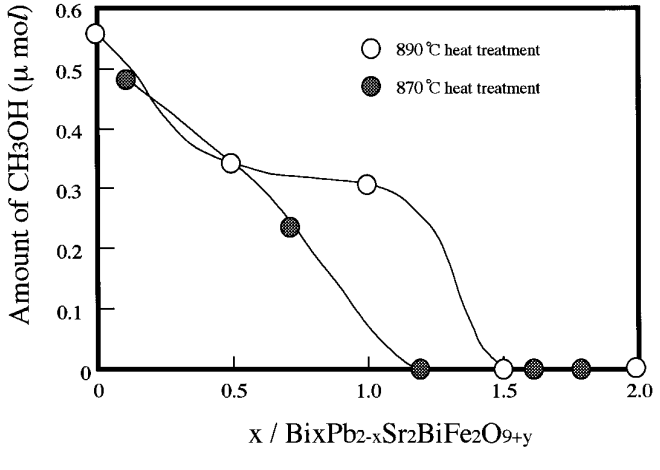

FIG. 11. Amount of CH_3OH photoproduced from CO_2 (4 h illumination time) as a function of x in $Bi_xPb_{2-x}Sr_2BiFe_2O_{9+y}$.

an element with a low electronegativity exists in the structure, and vice versa, while the bandgap is fixed if the element is not a transition metal. It was pointed out that the charge transfer sites depend on the band structure. The photoreduction of CO_2 to produce CH_3OH was observed on $CaFe_2O_4$ and $(Bi, Pb)_2Sr_2BiFe_2O_{9+y}$. The photocatalytic production of CH_3OH increased with an increase in the Pb content in the latter oxide. The elements constituting the oxides as well as the energy positions of the band edges were found to be important for the photocatalytic activity.

REFERENCES

1. L. A. Harris and R. H. Wilson, *Ann. Rev. Master. Sci.* **8,** 99 (1978).
2. M. A. Butler and D. S. Ginley, *J. Electrochem. Soc.* **125,** 228 (1978).
3. D. E. Scaife, *Solar Energy* **25,** 41 (1980).
4. J. Yoshimura, Y. Ebina, J. Kondo, K. Domen, and A. Tanaka, *J. Phys. Chem.* **97,** 1970 (1993).
5. Y. Matsumoto, M. Obata, and J. Hombo, *J. Phys. Chem.* **98,** 2950 (1994).
6. Y. Matsumoto, K. Suguyama, and E. Sato, *J. Solid State Chem.* **74,** 117 (1988)
7. Y. Matsumoto, M. Omae, I. Watanabe, and E. Sato, *J. Electrochem. Soc.* **133,** 711 (1986).
8. G. Campet, M. Jakani, J. P. Doumere, J. Claverie, and P. Hagenmuller, *Solid State Commun.* **42,** 93 (1982).
9. K. Kochev, K. Tzvetkova, and M. Gospodinov, *J. Electrochem. Soc.* **130,** 330 (1983).
10. J. Gautron, P. Lemasson, B. Poumellec, and J-F Marucco, *Solar Energy Mater.* **9,** 101 (1983).
11. D. S. Ginley and M. A. Butler, *J. Appl. Phys.* **48,** 2019 (1977).
12. H. Yoneyama, T. Ohkubo, and H. Tamura, *Bull. Chem. Soc. Jpn.* **54,** 404 (1981).
13. E. Pollert, J. Hejtmaneck, J. P. Doumerc, J. Claverie, and P. Hagenmuller, *J. Phys. Chem. Solid* **44,** 273 (1983).
14. M. A. Butler, D. S. Ginley, and M. Eibschutz, *J. Appl. Phys.* **48,** 3070 (1977).
15. H. H. Kung, H. S. Jarrett, A. W. Sleight, and A. Ferretti, *J. Appl. Phys.* **48,** 2463 (1977).
16. J. M. Bolts and M. S. Wrighton, *J. Phys. Chem.* **80,** 2641 (1976).
17. K. Kochev, K. Tzvetkova, and M. Gospodinov, *Mater. Res. Bull.* **8,** 915 (1983).
18. M. A. Butler, *J. Appl. Phys.* **48,** 1914 (1977).
19. N. Hatanaka, T. Kobayashi, H. Yonegawa, and H. Tamura, *Electrochem. Acta* **27,** 1129 (1982).
20. F. A. Benko, C. L. MacLaurin, and F. P. Koffyberg, *Mater. Res. Bull.* **17,** 133 (1982).
21. M. Metikos-Hukovic, *Electrochem. Acta* **26,** 981 (1981).
22. F-T. Liou, C. Y. Yang, and K. Hakin, *J. Appl. Electrochem.* **13,** 377 (1983).
23. J. F. McCann and A. Kham, *Electrochim. Acta* **27,** 89 (1982).
24. T. E. Phillips, K. Moorjani, J. C. Murphy, and T. O. Poeller, *J. Electrochem. Soc.* **129,** 1210 (1982).
25. K. L. Hardee and A. J. Bard, *J. Electrochem. Soc.* **124,** 215 (1977).
26. H. S. Jarrett, A. W. Sleight, H. H. Kung, and J. L. Gillson, *J. Appl. Phys.* **51,** 3916 (1980).
27. M. Metikos-Hukovic and B. Lovrecek, *Electrochim. Acta* **23,** 1371 (1978).
28. F. Lohmann, *Z. Naturforsch. Teil A* **22,** 843 (1967).
29. Y. Matsumoto, M. Omae, K. Sugiyama, and E. Sato, *J. Phys. Chem.* **91,** 577 (1987).
30. Y. Matsumoto, K. Sugiyama, and E. Sato, *J. Electrochem. Soc.* **135,** 98 (1988).
31. J. E. Turner, M. Hendewerk, J. Parmeter, D. Neiman, and G. A. Somorjai, *J. Electrochem. Soc.* **131,** 177 (1984).
32. A. H. A. Tinnemans, J. P. M. Koster, A. Makor, and J. Schoonman, *Ber. Bunsenges. Phys. Chem.* **90,** 390 (1986).
33. J. B. Goodenough, *in* "Progress in Solid State Chemistry" (H. Reiss, Ed.), Vol. 5, p. 145. Pergamon, Oxford, 1971.
34. I. Balberg and H. L. Pinch, *J. Magn. Magn. Mat.* **7,** 12 (1978).
35. Y. Matsumoto and E. Sato, *Mater. Chem. Phys.* **14,** 397 (1986).
36. Z. Coren, I. Willer, A. J. Nelson, and A. J. Frank, *J. Phys. Chem.* **94,** 3784 (1990).
37. S. Kemmler-Sack, A. Ehmann, T. Fries, G. Mayer-Von Kurthy, S. Losch, and M. Schlichenmaier, *J. Less-Common Met.* **153,** L31 (1989).
38. T. Fries, G. Mayer-Von Kurthy, A. Ehmann, S. Losch, M. Schlichenmaier, and S. Kemmler-Sack, *J. Less-Common Met.* **153,** L37 (1989).